Materials Science and Engineering B 213 (2016) 83–89

Contents lists available at ScienceDirect

Materials Science and Engineering B

journal homepage: www.elsevier.com/locate/mseb

Nitrogen-doped graphene nanosheets/sulfur composite as lithium–sulfur batteries cathode

Yong Hao[a], Xifei Li[b,c], Xueliang Sun[b,c], Chunlei Wang[a,*]

[a] Department of Mechanical and Materials Engineering, Florida International University, 10555 W. Flagler Street, Miami, FL 33174, USA
[b] Nanomaterials and Energy Lab, Department of Mechanical and Materials Engineering, Western University, London, Ontario N6A 5B9, Canada
[c] Energy and Materials Engineering Centre, College of Physics and Materials Science, Tianjin Normal University, Tianjin 300387, China

ARTICLE INFO

Article history:
Received 29 February 2016
Received in revised form 2 April 2016
Accepted 12 April 2016
Available online 23 April 2016

ABSTRACT

Lithium–sulfur batteries have been receiving unprecedented attentions in recent years due to their exceptional high theoretical capacity and energy density, low cost and environmental friendliness. Yet their practical applications are still hindered by short cycle life, low efficiency and poor conductivity which are mainly caused by the insulating nature of sulfur and dissolution of polysulfides. Here, a nitrogen-doped graphene nanosheets/sulfur (NGNSs/S) composite was synthesized via a facile chemical reaction deposition. In this composite, NGNSs was employed as a conductive host to entrap S/polysulfides in the cathode part. The NGNSs/S composite delivered an initial discharge capacity of 856.7 mAh g^{-1} and a reversible capacity of 319.3 mAh g^{-1} at 0.1 C with good recoverable rate capability.

1. Introduction

Recently lithium–sulfur (Li–S) batteries are becoming one of the most attractive next-generation lithium batteries. As one of the most abundant, low-cost and environmental friendly elements on earth, sulfur has a theoretical capacity and energy density of 1675 mAh g^{-1} and 2600 Wh kg^{-1} (vs. 272 mAh g^{-1} and 387 Wh kg^{-1} for $LiCoO_2$), respectively, which are much higher than typical commercial lithium-ion battery cathodes such as $LiCoO_2$, $LiMn_2O_4$ and $LiFePO_4$ [1,2]. However, low active material utilization, capacity degradation, poor Coulombic efficiency and poor cycle life are the challenges of Li–S cells using sulfur cathodes. During the electrochemical reaction, both sulfur and its discharge product Li_2S have high electrical resistivities [3]. Moreover, dissolution of polysulfides in the electrolyte and precipitation of polysulfides on the electrodes result in the so-called shuttle effect [4], which leads to the decrease of the active mass utilization during discharge process and strain field which degrades the cycle life [5–7]. It was also reported that volume expansion and crack formation of the sulfur electrodes take place during cycling which could lead to the failure of batteries [8]. In recent years, intensive efforts have been exerted in improving Li–S batteries by developing sulfur composite cathode materials (such as sulfur/carbon materials composite [9–13], sulfur/conductive polymers composite [14–17] and sulfur/metal oxide additives composite [18–20]), modifying electrolytes to manipulate the solubility of polysulfides (such as changing lithium salt and solvent [21,22], employing polymer electrolyte [23], adding electrolyte additive [24] and using polysulfides containing electrolyte [25,26]), and designing various cell configurations (such as placing carbon-based interlayer [27–30], coating modification of separator [31–33], fabricating lithium metal free anode [34], and binder or metal current collector free cathode [35–37]).

Graphene, a two-dimensional (2D) crystalline allotrope of carbon, has been considered as a promising conductive matrix for Li–S batteries due to its superior electrical conductivity, high specific surface area and excellent chemical tolerance. Graphene/sulfur composites with different structures such as graphene-wrapped sulfur particles [38–41] or sandwich type composites [42–44] have been reported. However, these close-type structures only provide physical barriers by which polysulfides dissolution in the electrolyte is hardly prevented in long term cycling and constrain Li^+ transporting across graphene in the lateral direction. Chemical adsorption of sulfur and polysulfides by the host is another attractive strategy to effectively eliminate the polysulfide dissolution. Several studies have been reported on the chemical interactions between functional group (e.g. oxygen group or hydroxyl group) on graphene and polysulfides which are beneficial to the enhancement of polysulfides immobilization [45,46]. Nitrogen- (N-) doping by introducing nitrogen groups and generating the extrinsic defects on carbon lattice is proved to be an effective way to improve the electrochemical performance of electrodes [47–54]. There are

* Corresponding author. Tel.: +1 305 348 1217.
E-mail address: wangc@fiu.edu (C. Wang).

http://dx.doi.org/10.1016/j.mseb.2016.04.009
0921-5107/

three major types of N-doped groups: pyridinic-N, pyrrolic-N and graphitic-N [55]. It has been found that these N-doped active sites can adsorb Li^+ and also serve as tunnels for Li^+ transportation [56]. Recently, several studies have been reported on developing N-doped graphene/sulfur (NG/S) composite for Li–S batteries. X. Wang et al. synthesized two types of NG/S composite: pyridinic-N enriched and pyrrolic-N enriched, respectively. Pyridinic-N has been proved to contribute more efficiently on confining the diffusion of soluble polysulfides [57]. In another work, C. Wang et al. reported a NG/S composite with 3D structure. The NG with the pyridinic-, pyrrolic- and graphitic-N groups exhibited a better performance comparing to undoped graphene, which was attributed to the 3D conductive network and reactive N functional groups [58]. Y. Qiu et al. further studied the role of N-doping in immobilizing polysulfides and compared the binding energies for primitive-, pyridine- and pyrrole-graphene with atomic Li and polysulfides by a computational method. It has been revealed that the enhancement is mainly due to the ionic attractions between N and Li cations, instead of N and S anions [59]. All the work above so far has been successfully introduced basic N functional groups in the NG sheets. It has to be noted that the performance of NG can be determined by several factors, such as the type of N functional groups, the N content in the NG, and structure and morphology of NG induced by N-doping, indicating more studies related to NG/S composites need to be further addressed.

In order to study the contribution of other N-doped functional groups, in this work, we have successfully synthesized the N-doped graphene nanosheets with amino-N and pyridine-N-oxide functional groups. The N-doped graphene nanosheets/sulfur (NGNSs/S) composite was prepared and evaluated as cathode materials in Li–S batteries. At 0.1 C, the NGNSs/S composite exhibited discharge capacities of 857 mAh g^{-1} and 319.3 mAh g^{-1} at the first and 20th circles, respectively. It is suggested that the NGNSs provided a conductive matrix with high surface area and high conductivity and N functional groups facilitated immobilization of the polysulfides.

2. Experimental

2.1. Synthesis of NGNSs

NGNSs were synthesized from natural flake graphite, as reported in our previous work [55,60]. First, graphite oxide was obtained by the oxidation of natural graphite in a modified Hummers method [55]. The graphene nanosheets (GNSs) were obtained by the thermal exfoliation of graphite oxide at 1050 °C for 30 s under nitrogen atmosphere. NGNSs were produced by treating the pristine GNSs at the mixed gas of ammonia and argon at 900 °C for 5 min [60].

2.2. Synthesis of NGNSs/S composite

NGNSs/S composite was synthesized by a facile chemical reaction deposition method [58]. The procedures are as illustrated in Fig. 1a. First, a 0.04 M $Na_2S_2O_3$ solution was prepared by dissolving 1.58 g $Na_2S_2O_3$ in 250 ml distilled water, followed by magnetic stirring for 30 min. Next, the as-synthesized 0.4 g NGNSs were dispersed in the $Na_2S_2O_3$ solution to produce composite. The mixture was under sonication for 1 h and it was continuously stirred. Then, 20 ml 10 M hydrochloric acid was dropped into the solution. After stirring for 24 h to let the reaction proceed completely, the product was filtered and washed with distilled water several times to eliminate salt products as well as until pH reached 7 and finally dried in a vacuum oven at 60 °C for 24 h. GNSs/S composite was synthesized by the same procedures as NGNSs/S composite. Pure S particles were obtained via the same chemical reaction route as described above and in the chemical Eq. (1) as below [61]:

$$Na_2S_2O_3 + 2HCl \rightarrow 2NaCl + SO_2\uparrow + H_2O + S\downarrow \quad (1)$$

2.3. Characterization

The microstructure and morphology characterization of obtained NGNSs, S particles and NGNSs/S composite was carried out by using a JEOL FE6330 field-emission scanning electron microscope (SEM). The nitrogen contents of NGNSs were determined by XPS analysis with a Kratos Axis Ultra Al (α) X-ray photoelectron spectroscopy at 14 kV. The crystal structures of the products were examined by X-ray diffraction (XRD) on a Siemens D5000 X-ray diffractometer via Cu Kα radiation between 10° and 90° at a scan rate of 2°/min. The surface area was characterized by nitrogen adsorption/desorption isotherms at 77 K using a Tri-Star II Micromeritics and calculated by Brunauer–Emmett–Teller (BET) measurement. Detailed surface information of NGNSs was obtained by using a JASCO Fourier transform-infrared spectrometer (FTIR)-4100. The weight percentage of sulfur in the composite was determined by thermogravimetric analysis (TGA) conducting on a SDT Q600 at a heating rate of 5 °C/min from room temperature to 400 °C under nitrogen protection.

2.4. Electrochemical measurement

Electrochemical characterization was carried out in CR2032-type coin cells. The NGNSs/S working electrodes were constructed from 80 wt.% NGNSs/S composite, 10 wt.% poly(vinylidene difluoride) (PVDF) binder, and 10 wt.% Carbon black in an N-methyl-2-pyrrolidinone (NMP) solution. GNSs/S, sulfur particles and NGNSs working electrodes were also prepared and evaluated as control samples. The well mixed slurry was uniformly casted onto aluminum foil current collectors and the electrodes were dried in a vacuum oven at 60 °C for 12 h. The coin cells were assembled in an argon-filled glove box with lithium metals as the counter and reference electrodes and Celgard 2400 polypropylene film was used as separator. The electrolyte was a 1 M lithium bis(trifluoromethanesulfonyl)imide (LiTFSI) in 1,2-dimethoxyethane (DME) and 1,3-dioxolane (DOL) (1:1, v/v) with 1 wt.% $LiNO_3$ mixed solution. The cyclic voltammetry (CV) data were collected with a biologic VMP3 potentiostat at a scan rate of 0.1 mV s^{-1} at 1.0–3.0 V (vs. Li/Li^+). Galvanostatic charge/discharge cycling profiles of the cells with constant current densities and rate capability at various current densities were conducted at a cut-off potential of 1.0–3.0 V (vs. Li/Li^+) on a Neware BTS-610 instrument. Electrochemical impedance spectroscopy (EIS) was conducted on the VMP3 in the frequency range from 100 kHz to 0.1 Hz with an input AC voltage amplitude of 10 mV. All the electrochemical tests were performed at room temperature.

3. Results and discussion

3.1. Characterization

The SEM results of S particle, NGNSs and NGNSs/S composite are compared in Fig. 1b–d. It can be seen in Fig. 1b that irregular shaped sulfur particles formed by precipitation of chemical reaction are in the particle size of several microns. Fig. 1c displays the morphology of NGNSs which was randomly orientated agglomerate of planar sheets. Fig. 1d shows the morphologies of NGNSs/S composite at different magnifications. It can be observed that the sulfur particles are pretty homogenously mixed with the NGNSs together (Fig. 1d inset). Fig. 1e shows the TEM image of NGNSs, in which the 2D layered structure of NGNSs can be observed.

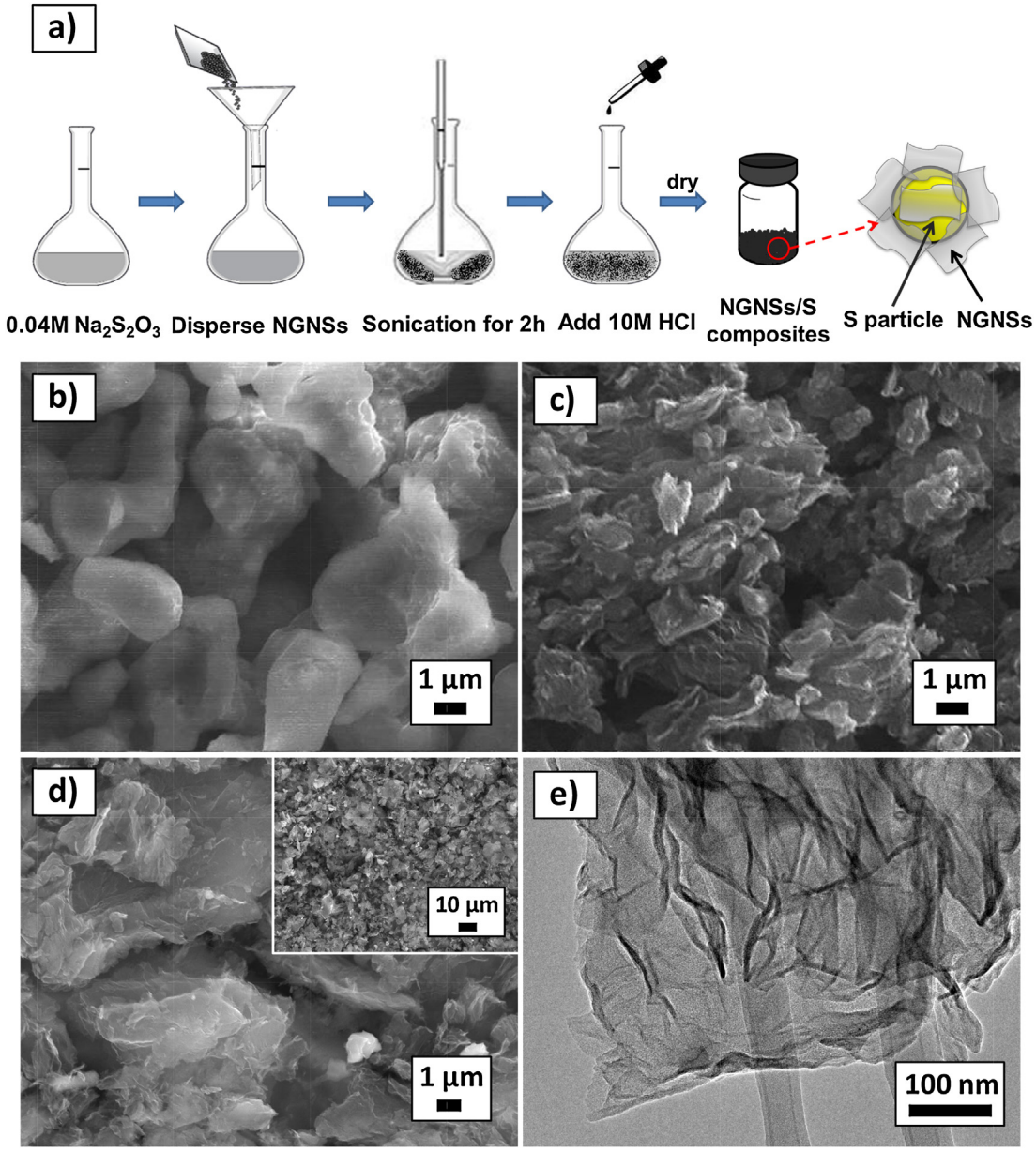

Fig. 1. (a) Illustration of synthesis process of NGNSs/S composite; SEM images of (b) S particles, (c) NGNSs, (d) NGNSs/S composite (inset at low magnification) and (e) a typical TEM image of NGNSs.

XPS was applied for analyzing the surface chemistry and measuring the elemental composition of NGNSs. Fig. 2a shows XPS analysis spectrum of NGNSs. It can be seen that there is one sharp peak at 284.35 eV, corresponding to C 1s as expected. The peak at 399.15 eV represents N 1s, indicating nitrogen has been successfully doped in the NGNSs. Besides the presence of C1s and N1s, O1s peaks at 532.85 eV can also be observed in the XPS spectrum of NGNSs. The relative atomic percentages of C 1s, N 1s and O 1s are calculated from the XPS spectrum as 95.5%, 1.2% and 3.3%, respectively. The coverage of N on the graphene surface could be estimated as about 1.3%. The XPS N 1s spectrum of NGNSs is shown in Fig. 2b. It can be observed there are two fitting peaks in the N 1s spectrum with binding energies of 399.02 eV and 402.10 eV, corresponding to amino-N and pyridine-N-oxide, respectively [49,62].

The XRD patterns of elemental sulfur particles, NGNSs and as-synthesized NGNSs/S composite are presented in Fig. 3a. It is observed that the pristine NGNSs exists two broad diffraction peaks around 26° and 42°, corresponding to the general characteristic (002) and (100) diffraction peaks of multi-layered graphene. The XRD pattern of elemental sulfur particles generally exhibits a series of sharp and strong peaks, indicating a well-defined Fddd orthorhombic crystalline structure of sulfur (JCPDS#: 08-0247). The XRD pattern of NGNSs/S composite shows most sharp and strong sulfur peaks as well, indicating the existing of sulfur in the composite. The broad peaks of NGNSs are barely obvious in the NGNSs/S composite with sulfur loading. Fig. 3b shows the surface area measurement results of NGNSs and NGNSs/S composite. For NGNSs, the surface area is around 330 $m^2 g^{-1}$. After sulfur loading, the surface area of NGNSs/S composite turns out to be 10 $m^2 g^{-1}$. This massive decrease after sulfur loading reveals that the loading of sulfur particles occupies the most surface area of NGNSs [50].

The nitrogen functionalization on NGNSs was also characterized by FTIR, as shown in Fig. 3c. It can be seen that there is a board band centered at 2340 cm^{-1}, indicating the presence of adsorbed CO_2 and/or vibration of C=N=O asymmetric stretching [53]. The

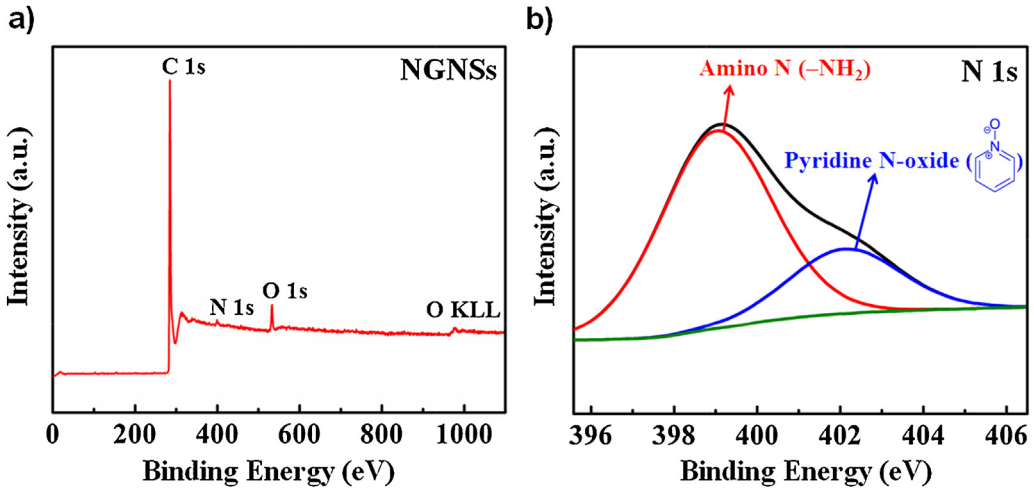

Fig. 2. XPS spectra of NGNSs: (a) wide scan and (b) N 1s.

vibration peaks at ~1530 cm^{-1} and ~1670 cm^{-1} can be indexed to amine groups of N—H stretching and scissoring [53,63]. The FTIR matches the obtained results of XPS analysis and further confirms that nitrogen has been successfully doped into graphene structure. TGA was conducted on as-synthesized NGNSs/S sample and the result is shown in Fig. 3d. The NGNSs/S composite has a weight loss of 45 wt.% with the temperature increasing from 150 to 250 °C, indicating that there is a content of 45 wt.% sulfur in the NGNSs/S composite.

3.2. Electrochemical properties

The electrochemical properties of NGNSs/S composite were investigated as shown in Fig. 4. Fig. 4a shows the cyclic

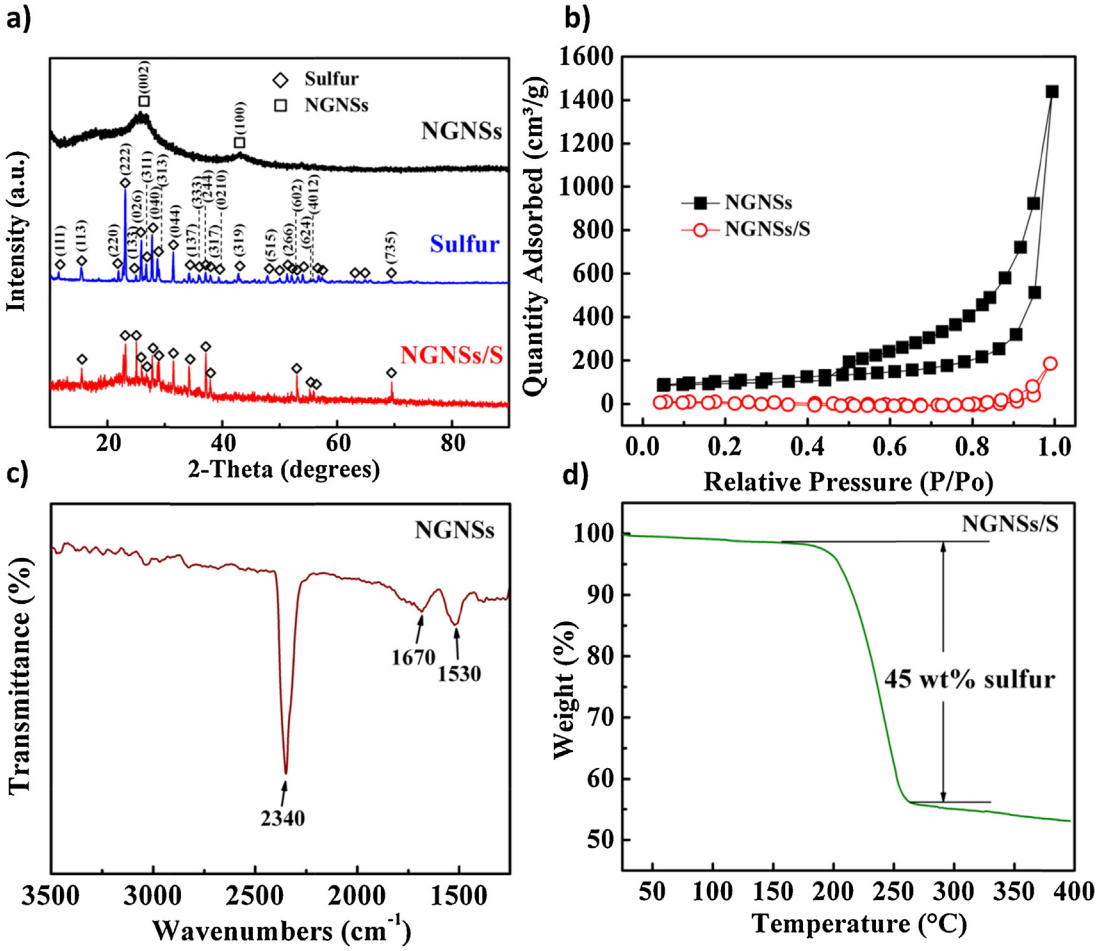

Fig. 3. (a) XRD patterns of sulfur, NGNSs and NGNSs/S composite, (b) N_2 adsorption–desorption isotherms of NGNSs and NGNSs/S composite, (c) FTIR spectra of NGNSs and (d) TGA analysis of NGNSs/S composite.

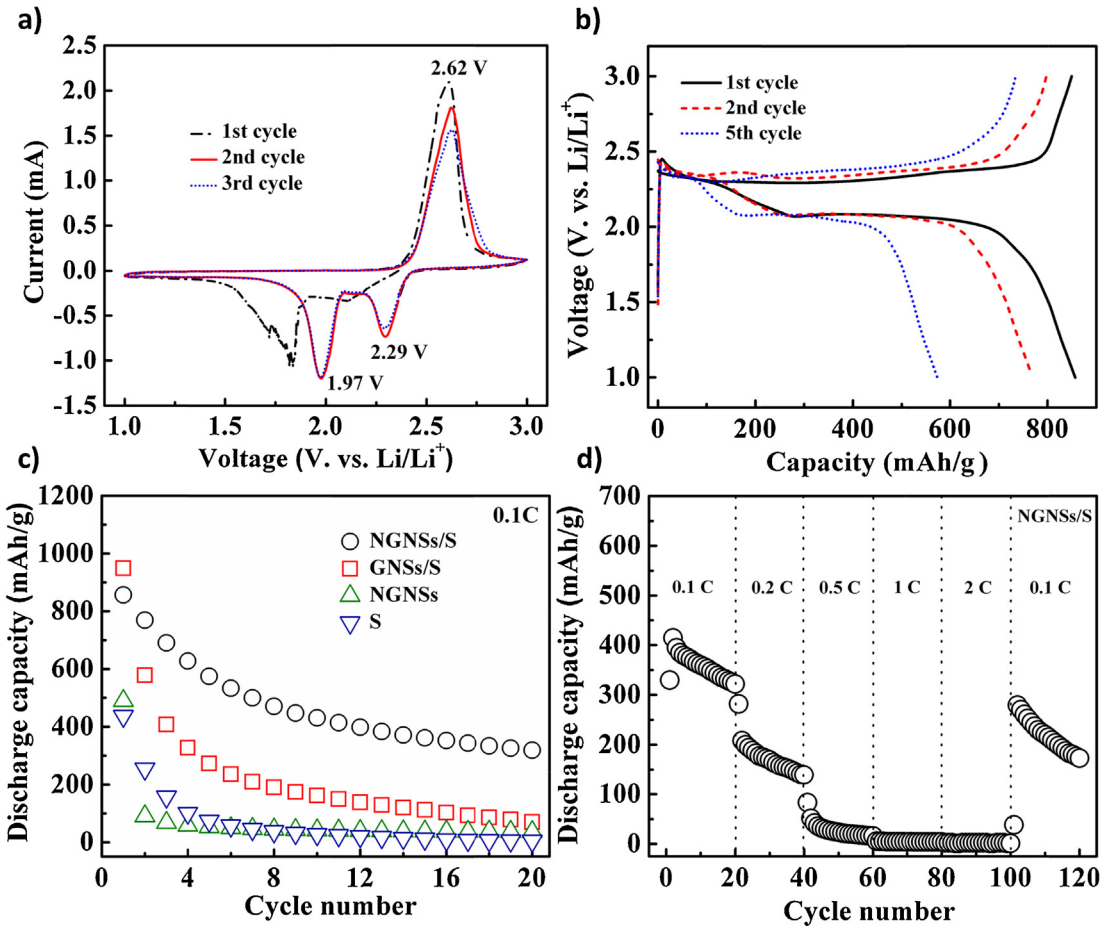

Fig. 4. (a) Cyclic voltammograms of NGNSs/S composite as working electrode at a scan rate of 0.1 mV s^{-1} between 1.0 and 3.0 V (vs. Li/Li^+), (b) the 1st, 2nd and 5th cycles of discharge/charge profile of NGNSs/S composite at 0.1 C, (c) cycling performances of NGNSs/S composite, GNSs/S composite, NGNSs and S at 0.1 C and (d) rate performance of NGNSs/S composite at various rates.

voltammetry (CV) profiles of the NGNSs/S cathode for the initial 1st, 2nd and 3rd cycles between 1.0 and 3.0 V (vs. Li/Li^+). In the cathodic scan of the first cycle, the NGNSs/S electrode exhibits a small shoulder at 2.11 V and a broad peak starting at 1.83 V. The small shoulder around 2.11 V could be assigned to the formation of soluble polysulfides (Li_2S_x, $4 \leq x \leq 8$) during lithiation, while the low voltage peak around 1.83 V is most likely associated to the formation of insoluble lithium disulfide Li_2S_2 and lithium sulfide Li_2S [51]. During the anodic process, there is only one oxidation peak observed and 2.62 V (vs. Li/Li^+). This can be assigned to delithiation process of Li_2S back to polysulfides and eventually to S [57]. In the second and third cycle, there are two reduction peaks observed at 2.29 V and 1.97 V, which shift toward more positive direction in comparison to the first cycle. The change of kinetics after the polysulfides formation could be related to the voltage shift. Meanwhile, similar voltage shift behavior was also reported and attributed to strain/stress generation during polysulfides formation [64]. Further study needs to be conducted to clarify the voltage shift mechanism. For the oxidation peaks in the second and third cycle, the currents of the peaks decrease which may be due to the dissolution of polysulfides. Fig. 4b shows the galvanostatic charge/discharge curves of NGNSs/S composite cathode at the 1st, 2nd and 5th cycles. The first discharge curve suggests that there are two plateaus which correspond well with two apparent reduction peaks in CV results. The first plateau observed at 2.3 V is attributed to the formation of soluble polysulfides. The second plateau at 2.1 V corresponds to the reduction of soluble polysulfides to insoluble Li_2S_2 and Li_2S. In the following cycles, the discharge processes follow the steps as the first cycle. From the first charge curve, it can be observed that there is a sharp rise at the beginning and follow by a shallow dip. The initial sharp rise is due to the polarization of Li_2S passivation layer on the surface of cathode and the shallow dip may be attributed to the depolarization of insoluble Li_2S to soluble polysulfides by electrochemical oxidation [6,65]. The one major plateau is assigned to the oxidation of polysulfides to element S [7,66]. Based on the CV and charge/discharge profiles, the reaction occurring at NGNSs/S cathode during discharge proceeds through a series of steps can be described as below (Eqs. (2)–(6)) [67,68].

$$S_8 + 2e^- \rightarrow S_8^{2-} \quad (2)$$

$$3S_8^{2-} + 2e^- \rightarrow 4S_6^{2-} \quad (3)$$

$$2S_6^{2-} + 2e^- \rightarrow 3S_4^{2-} \quad (4)$$

$$S_4^{2-} + 4Li^+ + 2e^- \rightarrow 2Li_2S_2 \quad (5)$$

$$Li_2S_2 + 2Li^+ + 2e^- \rightarrow 2Li_2S \quad (6)$$

Fig. 4c compares the cycling performance of the NGNSs/S composite, control samples GNSs/S composite, NGNSs and S (CV and charge/discharge profiles of NGNSs and S are shown in Figs. S1 and S2, respectively) at a current rate of 0.1 C. The NGNSs/S shows a discharge capacity of 856.7 mAh g^{-1} in the first cycle which is higher than the capacity of 489.9 mAh g^{-1} of NGNSs and capacity of 437.1 mAh g^{-1} of S. The capacity of NGNSs/S fades to 319.2 mAh g^{-1} after 20 cycles while the capacity of bare sulfur electrode decreases to 4.1 mAh g^{-1}. Although the GNSs/S exhibits the first discharge capacity of 949.2 mAh g^{-1}, the capacity fades faster

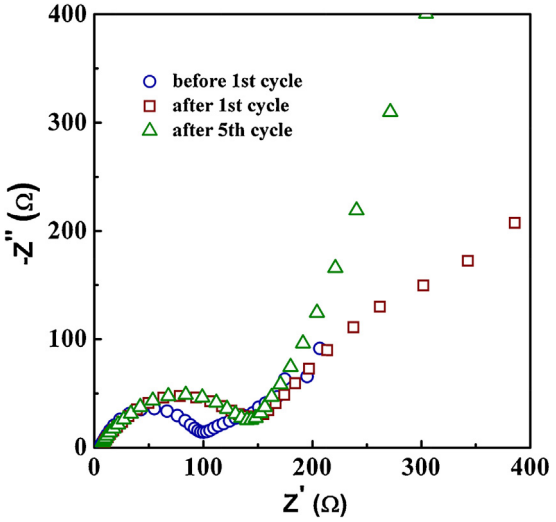

Fig. 5. Nyquist plots of the Li–S cell with NGNSs/S composite cathode before the 1st, after the 1st and 5th cycles.

compared to the NGNSs/S composite and decreases to 69.3 mAh g^{-1} at the 20th cycle. The enhanced cycling performance could be attributed to the N-doped functional groups, which has beneficial effect on the confinement of polysulfides in the NGNSs/S composite. However, the capacity fading with cycling still can be observed due to the polysulfides inevitably dissolving into the electrolyte. Fig. 4d shows the rate performance of NGNSs/S at various C rates. The 20th cycle discharge capacities are 321.8, 139.0, 15.9, 4.1, 1.2 and 173.0 mAh g^{-1}, respectively, at discharge rates of 0.1, 0.2, 0.5, 1, 2 and 0.1 C, respectively. For each rate performance, it can be seen that there is capacity fading during the cycling performance which may due to the polysulfides dissolve into the electrolyte discussed above. However, it is noticed that when the rate turns back to 0.1 C, the specific capacity recovers to 173.0 mAh g^{-1}, indicating that NGNSs/S composite still presents a good rate capability. It has to be noted that there are only few published Li–S works using NGNSs/S composite. The enhanced electrochemical performance so far was mainly attributed to the three common types of N-doped functional groups, which are pyridinic-N, pyrrolic-N and graphitic-N. In this work, we demonstrated that the NGNSs with amino-N and pyridine-N-oxide can also contribute to the enhancement of the electrochemical performance in Li–S cells. We believe that the electrochemical performance can be further improved by modifying the coverage of N-doped functional groups, which needs to be investigated in the future work.

To further investigate charge transfer resistance of NGNSs/S composite cathode during cycling, EIS of Li–S cell before and after the 1st cycle (i.e., test at the end of the 1st cycle), and after the 5th cycle (i.e., test at the end of the 5th cycle) were conducted, as shown in Fig. 5. The impedance plots are composed of one semicircle in the high frequency region and near linear line in the low frequency region. The semicircles are assigned to the solid-electrolyte interface resistance and the charge transfer resistance of the NGNSs/S electrode. It can be seen that radii of the semicircles after the 1st and 5th cycles are larger than the radius before cycling, indicating that charge transfer kinetics become lower which may be due to the resistance of the irreversible deposition and aggregation of insulated Li_2S_2/Li_2S layer on the surface of NGNSs/S electrode after cycling. The resistance of NGNSs/S changes from about 100 Ω before the 1st cycle to about 150 Ω in the following cycles. However, the semicircle radii after the 1st and 5th cycles are almost unchanged, which implies that NGNSs/S cathode achieves a stable interfacial charge-transfer process during cycling [52]. The linear line relates to the diffusion kinetics of Li^+ within the electrodes. It can be seen that the slope of the linear line after 5th cycle turns to be steeper compared to the slopes before and after the 1st cycle, which indicates NGNSs/S cathode is in favor of rapid Li^+ transport with cycling.

4. Conclusion

In summary, the NGNSs/S composite has been successfully synthesized by a facile chemical reaction deposition method. The NGNSs/S cathode exhibits good rate capability and good specific discharge capacity of 319.3 mAh g^{-1} at 0.1 C after 20 cycles. The NGNSs apply as a framework formed by the 2D graphene layer could anchor sulfur particles, improve the conductivity of the electrode and enlarge the contact surface area to allow fast Li^+ transport.

Acknowledgments

This work is partially supported by the National Science Foundation (NSF) projects (no. 1506640 and no. 1509735) and NERC ASSIST center seed funding. Y. Hao acknowledges Doctoral Evidence Acquisition (DEA) fellowship from UGS at FIU and facilities of AMERI at FIU.

Appendix A. Supplementary data

Supplementary data associated with this article can be found, in the online version, at http://dx.doi.org/10.1016/j.mseb.2016.04.009.

References

[1] Y.X. Yin, S. Xin, Y.G. Guo, L.J. Wan, Angew. Chem. Int. Ed. 52 (2013) 13186–13200.
[2] B. Papandrea, X. Xu, Y. Xu, C.-Y. Chen, Z. Lin, G. Wang, Y. Luo, M. Liu, Y. Huang, L. Mai, Nano Res. 9 (2016) 240–248.
[3] Y. Fu, C. Zu, A. Manthiram, J. Am. Chem. Soc. 135 (2013) 18044–18047.
[4] J.-Q. Huang, Q. Zhang, H.-J. Peng, X.-Y. Liu, W.-Z. Qian, F. Wei, Energy Environ. Sci. 7 (2014) 347–353.
[5] R. Elazari, G. Salitra, Y. Talyosef, J. Grinblat, C. Scordilis-Kelley, A. Xiao, J. Affinito, D. Aurbach, J. Electrochem. Soc. 157 (2010) A1131–A1138.
[6] S.S. Zhang, J. Power Sources 231 (2013) 153–162.
[7] N.A. Cañas, S. Wolf, N. Wagner, K.A. Friedrich, J. Power Sources 226 (2013) 313–319.
[8] Y. Yang, G. Zheng, Y. Cui, Chem. Soc. Rev. 42 (2013) 3018–3032.
[9] T. Lin, Y. Tang, Y. Wang, H. Bi, Z. Liu, F. Huang, X. Xie, M. Jiang, Energy Environ. Sci. 6 (2013) 1283–1290.
[10] J.-Q. Huang, Q. Zhang, S.-M. Zhang, X.-F. Liu, W. Zhu, W.-Z. Qian, F. Wei, Carbon 58 (2013) 99–106.
[11] X.A. Chen, Z. Xiao, X. Ning, Z. Liu, Z. Yang, C. Zou, S. Wang, X. Chen, Y. Chen, S. Huang, Adv. Energy Mater. 4 (2014) 1301988.
[12] X. Li, X. Li, M.N. Banis, B. Wang, A. Lushington, X. Cui, R. Li, T.-K. Sham, X. Sun, J. Mater. Chem. A 2 (2014) 12866–12872.
[13] X. Li, Q. Sun, J. Liu, B. Xiao, R. Li, X. Sun, J. Power Sources 302 (2016) 174–179.
[14] J. Fanous, M. Wegner, J. Grimminger, A.N. Andresen, M.R. Buchmeiser, Chem. Mater. 23 (2011) 5024–5028.
[15] Y. Zhang, Z. Bakenov, Y. Zhao, A. Konarov, T.N.L. Doan, M. Malik, T. Paron, P. Chen, J. Power Sources 208 (2012) 1–8.
[16] W. Zhou, Y. Yu, H. Chen, F.J. DiSalvo, H.C.D. Abruña, J. Am. Chem. Soc. 135 (2013) 16736–16743.
[17] W. Li, Q. Zhang, G. Zheng, Z.W. Seh, H. Yao, Y. Cui, Nano Lett. 13 (2013) 5534–5540.
[18] X. Ji, S. Evers, R. Black, L.F. Nazar, Nat. Commun. 2 (2011) 325.
[19] S. Evers, T. Yim, L.F. Nazar, J. Phys. Chem. C 116 (2012) 19653–19658.
[20] Z.W. Seh, W. Li, J.J. Cha, G. Zheng, Y. Yang, M.T. McDowell, P.-C. Hsu, Y. Cui, Nat. Commun. 4 (2013) 1331.
[21] C. Barchasz, J.-C. Leprêtre, S. Patoux, F. Alloin, J. Electrochem. Soc. 160 (2013) A430–A436.
[22] L. Suo, Y.-S. Hu, H. Li, M. Armand, L. Chen, Nat. Commun. 4 (2013) 1481.
[23] J. Jin, Z. Wen, X. Liang, Y. Cui, X. Wu, Solid State Ion. 225 (2012) 604–607.
[24] Z. Lin, Z. Liu, W. Fu, N.J. Dudney, C. Liang, Adv. Funct. Mater. 23 (2013) 1064–1069.
[25] D.J. Lee, M. Agostini, J.W. Park, Y.K. Sun, J. Hassoun, B. Scrosati, ChemSusChem 6 (2013) 2245–2248.
[26] S. Chen, F. Dai, M.L. Gordin, D. Wang, RSC Adv. 3 (2013) 3540–3543.
[27] Y.-S. Su, A. Manthiram, Nat. Commun. 3 (2012) 1166.

[28] Y.-S. Su, A. Manthiram, Chem. Commun. 48 (2012) 8817–8819.
[29] C. Zu, Y.-S. Su, Y. Fu, A. Manthiram, Phys. Chem. Chem. Phys. 15 (2013) 2291–2297.
[30] R. Singhal, S.-H. Chung, A. Manthiram, V. Kalra, J. Mater. Chem. A 3 (2015) 4530–4538.
[31] I. Bauer, S. Thieme, J. Brückner, H. Althues, S. Kaskel, J. Power Sources 251 (2014) 417–422.
[32] J. Balach, T. Jaumann, M. Klose, S. Oswald, J. Eckert, L. Giebeler, Adv. Funct. Mater. 25 (2015) 5285–5291.
[33] U. Stoeck, J. Balach, M. Klose, D. Wadewitz, E. Ahrens, J. Eckert, L. Giebeler, J. Power Sources 309 (2016) 76–81.
[34] J. Hassoun, J. Kim, D.-J. Lee, H.-G. Jung, S.-M. Lee, Y.-K. Sun, B. Scrosati, J. Power Sources 202 (2012) 308–313.
[35] R. Demir-Cakan, M. Morcrette, F. Nouar, C. Davoisne, T. Devic, D. Gonbeau, R. Dominko, C. Serre, G. Férey, J.-M. Tarascon, J. Am. Chem. Soc. 133 (2011) 16154–16160.
[36] H. Yao, G. Zheng, P.-C. Hsu, D. Kong, J.J. Cha, W. Li, Z.W. Seh, M.T. McDowell, K. Yan, Z. Liang, Nat. Commun. 5 (2014) 3943.
[37] S. Thieme, J. Brückner, I. Bauer, M. Oschatz, L. Borchardt, H. Althues, S. Kaskel, J. Mater. Chem. A 1 (2013) 9225–9234.
[38] H. Wang, Y. Yang, Y. Liang, J.T. Robinson, Y. Li, A. Jackson, Y. Cui, H. Dai, Nano Lett. 11 (2011) 2644–2647.
[39] S. Evers, L.F. Nazar, Chem. Commun. 48 (2012) 1233–1235.
[40] N. Li, M. Zheng, H. Lu, Z. Hu, C. Shen, X. Chang, G. Ji, J. Cao, Y. Shi, Chem. Commun. 48 (2012) 4106–4108.
[41] Y. Liu, J. Guo, J. Zhang, Q. Su, G. Du, Appl. Surf. Sci. 324 (2015) 399–404.
[42] Y. Cao, X. Li, I.A. Aksay, J. Lemmon, Z. Nie, Z. Yang, J. Liu, Phys. Chem. Chem. Phys. 13 (2011) 7660–7665.
[43] Y.-X. Wang, L. Huang, L.-C. Sun, S.-Y. Xie, G.-L. Xu, S.-R. Chen, Y.-F. Xu, J.-T. Li, S.-L. Chou, S.-X. Dou, J. Mater. Chem. 22 (2012) 4744–4750.
[44] R. Chen, T. Zhao, J. Lu, F. Wu, L. Li, J. Chen, G. Tan, Y. Ye, K. Amine, Nano Lett. 13 (2013) 4642–4649.
[45] L. Ji, M. Rao, H. Zheng, L. Zhang, Y. Li, W. Duan, J. Guo, E.J. Cairns, Y. Zhang, J. Am. Chem. Soc. 133 (2011) 18522–18525.
[46] C. Zu, A. Manthiram, Adv. Energy Mater. 3 (2013) 1008–1012.
[47] K. Chang, D. Geng, X. Li, J. Yang, Y. Tang, M. Cai, R. Li, X. Sun, Adv. Energy Mater. 3 (2013) 839–844.
[48] L.-S. Zhang, X.-Q. Liang, W.-G. Song, Z.-Y. Wu, Phys. Chem. Chem. Phys. 12 (2010) 12055–12059.
[49] Z. Wen, X. Wang, S. Mao, Z. Bo, H. Kim, S. Cui, G. Lu, X. Feng, J. Chen, Adv. Mater. 24 (2012) 5610–5616.
[50] X.G. Sun, X. Wang, R.T. Mayes, S. Dai, ChemSusChem 5 (2012) 2079–2085.
[51] F. Sun, J. Wang, H. Chen, W. Li, W. Qiao, D. Long, L. Ling, ACS Appl. Mater. Interfaces 5 (2013) 5630–5638.
[52] J. Yang, J. Xie, X. Zhou, Y. Zou, J. Tang, S. Wang, F. Chen, L. Wang, J. Phys. Chem. C 118 (2014) 1800–1807.
[53] P. Zhu, J. Song, D. Lv, D. Wang, C. Jaye, D.A. Fischer, T. Wu, Y. Chen, J. Phys. Chem. C 118 (2014) 7765–7771.
[54] J. Song, T. Xu, M.L. Gordin, P. Zhu, D. Lv, Y.B. Jiang, Y. Chen, Y. Duan, D. Wang, Adv. Funct. Mater. 24 (2014) 1243–1250.
[55] X. Li, D. Geng, Y. Zhang, X. Meng, R. Li, X. Sun, Electrochem. Commun. 13 (2011) 822–825.
[56] H.M. Jeong, J.W. Lee, W.H. Shin, Y.J. Choi, H.J. Shin, J.K. Kang, J.W. Choi, Nano Lett. 11 (2011) 2472–2477.
[57] X. Wang, Z. Zhang, Y. Qu, Y. Lai, J. Li, J. Power Sources 256 (2014) 361–368.
[58] C. Wang, K. Su, W. Wan, H. Guo, H. Zhou, J. Chen, X. Zhang, Y. Huang, J. Mater. Chem. A 2 (2014) 5018–5023.
[59] Y. Qiu, W. Li, W. Zhao, G. Li, Y. Hou, M. Liu, L. Zhou, F. Ye, H. Li, Z. Wei, Nano Lett. 14 (2014) 4821–4827.
[60] Y. Li, J. Wang, X. Li, D. Geng, M.N. Banis, R. Li, X. Sun, Electrochem. Commun. 18 (2012) 12–15.
[61] R.G. Chaudhuri, S. Paria, J. Colloid Interface Sci. 343 (2010) 439–446.
[62] C. Zhang, R. Hao, H. Liao, Y. Hou, Nano Energy 2 (2013) 88–97.
[63] D. Geng, S. Yang, Y. Zhang, J. Yang, J. Liu, R. Li, T.-K. Sham, X. Sun, S. Ye, S. Knights, Appl. Surf. Sci. 257 (2011) 9193–9198.
[64] S. Zheng, F. Yi, Z. Li, Y. Zhu, Y. Xu, C. Luo, J. Yang, C. Wang, Adv. Funct. Mater. 24 (2014) 4156–4163.
[65] C. Barchasz, F. Molton, C. Duboc, J.-C. Leprêtre, S. Patoux, F. Alloin, Anal. Chem. 84 (2012) 3973–3980.
[66] S. Xiong, X. Kai, X. Hong, Y. Diao, Ionics 18 (2012) 249–254.
[67] K. Kumaresan, Y. Mikhaylik, R.E. White, J. Electrochem. Soc. 155 (2008) A576–A582.
[68] S. Chen, X. Huang, H. Liu, B. Sun, W. Yeoh, K. Li, J. Zhang, G. Wang, Adv. Energy Mater. 4 (2014) 1301761.